

Article

Strongly Enhancing Photocatalytic Activity of TiO₂ Thin Films by Multi-Heterojunction Technique

Hsyi-En Cheng ¹, Chi-Hsiu Hung ², Ing-Song Yu ³ and Zu-Po Yang ^{2,*}

¹ Department of Electro-Optical Engineering, Southern Taiwan University of Science and Technology, Tainan 710, Taiwan; sean@stust.edu.tw

² Institute of Photonic System, National Chiao Tung University, Tainan 71150, Taiwan; cfv8248@gmail.com

³ Department of Materials Science and Engineering, National Dong Hwa University, Hualien 97401, Taiwan; isyu@gms.ndhu.edu.tw

* Correspondence: zupoyang@nctu.edu.tw; Tel.: +886-6-3032121 (ext. 57762)

Received: 13 September 2018; Accepted: 3 October 2018; Published: 6 October 2018



Abstract: The photocatalysts of immobilized TiO₂ film suffer from high carrier recombination loss when compared to its powder form. Although the TiO₂ with rutile-anatase mixed phases has higher carrier separation efficiency than those with pure anatase or rutile phase, the single junction of anatase/rutile cannot avoid the recombination of separated carriers at the interface. In this study, we propose a TiO₂/SnO₂/Ni multi-heterojunction structure which incorporates both Schottky contact and staggered band alignment to reduce the carrier recombination loss. The low carrier recombination rate of TiO₂ film in TiO₂/SnO₂/Ni multi-heterojunction structure was verified by its low photoluminescence intensity. The faster degradation of methylene blue for TiO₂/SnO₂/Ni multi-junctions than for the other fabricated structures, which means that the TiO₂ films grown on the SnO₂/Ni/Ti coated glass have a much higher photocatalytic activity than those grown on the blank glass, SnO₂-coated and Ni/Ti-coated glasses, demonstrated its higher performance of photogenerated carrier separation.

Keywords: multijunction; titanium dioxide; thin film; photocatalysis; functional coatings

1. Introduction

Titanium dioxide, TiO₂, is an inexpensive, non-toxic and chemically stable material. Its high refractive index and transparency for visible light have made it a widely used painting material, and its biological properties have made it a promising material for biomedical applications [1–3]. Recently, its strong oxidizing power under ultraviolet (UV) irradiation attracts great attention due to the applications of antibacterial, deodorizing, and remediation of environmental pollutions [4–10]. TiO₂ has a conduction band edge potential lower than that of hydrogen revolution and valence band edge potential higher than that of oxygen revolution. Therefore, in addition to decomposing the organic pollutions, the photogenerated electrons and holes in TiO₂ can be used to split water into hydrogen and oxygen directly [11]. A lot of studies on the properties of TiO₂ photocatalysts for water treatment or water splitting have been conducted [12–18]. Generally, TiO₂ in particulate form possesses higher photocatalytic performance due to its large surface area. It was found that the TiO₂ particulates with mixed-phase structure of anatase and rutile exhibit the best photocatalytic activity, followed by with the pure anatase phase, and then with the pure rutile phase. A high photocatalytic efficiency photocatalyst of TiO₂ powder called P-25 (Degussa) has been developed based on the mixture of anatase and rutile phases [19]. Unfortunately, precipitating and recovering the TiO₂ particulates from water limits its widespread use. In contrast, immobilized TiO₂ film is more practical because of its

controllability. Therefore, the way to improve the photocatalytic performance of immobilized TiO₂ films is urgently pursued.

The problem with the immobilized TiO₂ films is the high carrier recombination rate of TiO₂, which results in a low effective thickness for converting photon energy into chemical energy. Luttrell et al. [20] pointed out that the bulk transport ability of excitons to the surface dominates the photocatalytic activity of TiO₂ films. Their studies on the photodegradation of methyl orange demonstrated that the photocatalytic activity of TiO₂ films increases with the film thickness but reaches a maximum at ~2.5 nm for rutile and ~5 nm for anatase. This means that the carriers generated deeper than 2.5 nm and 5 nm for rutile and anatase, respectively, contribute little to the photodegradation of methyl orange. However, the thickness of 5 nm is too small when absorbing the incident light. The optical absorption coefficient of anatase TiO₂ in the near-UV region is rather low due to its indirect bandgap nature. The thickness required for anatase film to absorb 50% of the incident light with a wavelength of 340 nm has been reported to be around 500 nm [21]. Therefore, most of the incident lights pass through the 5 nm anatase film. Even if we thicken the film to absorb more incident photons, the carriers generated deeper than 5 nm from the surface cannot migrate to the surface for utilization. Therefore, the immobilized TiO₂ films suffer from either low photon absorption efficiency or high carrier recombination loss.

A variety of strategies have been adopted to enhance the photocatalytic activity of immobilized TiO₂ films. The most frequently investigated strategy involves growing a porous structure like a nanotube, nanopillar, nanorod, nanosheet, nanoflake or nanobelt arrays [22–30]. Although a porous structure can provide more reaction surface area for photocatalysis, it still cannot overcome the issue of low carrier transport ability. An alternative method which involves loading metal nanoparticles, e.g., platinum, gold or silver [31–37], on TiO₂ can create an electric field across the interface to facilitate the separation of photogenerated electron-hole pairs. Thus, the carrier transport in TiO₂ is improved by the prolonged carrier lifetime. As a consequence, the photocatalytic activity of TiO₂ films is enhanced. In our previous study [38], we grew TiO₂ films on Ni, Ta, and Ti coated glass substrates and found that the TiO₂ films on the Ni-coated substrate performs the highest photocatalytic activity, followed by on the Ti-coated substrate, and then on the Ta-coated substrate, the same as the sequence of their electron work function of Ni ~5.04–5.35 eV, Ti 4.33 eV, and Ta 4.00–4.15 eV [39]. This is because the high work function metals like platinum, gold, silver or nickel can attract the photogenerated electrons from TiO₂ as they come into contact with TiO₂, leading to a decrease of carrier recombination loss.

Nevertheless, the photogenerated holes in TiO₂ adjacent to the filled states of metal can also possibly cross into the metal to recombine with the electrons. Hence, introducing a semiconductor layer with an appropriate energy band structure in between the metal and TiO₂ is considered to be a feasible method for alleviating the recombination issue because the built energy barrier from the heterojunction between semiconductor and TiO₂ can block the holes in TiO₂ from entering the semiconductor and the metal. A similar concept of multi-heterojunction has been applied on the photo-induced hydrophilic conversion for TiO₂/WO₃ systems by Miyauchi et al [40]. The rutile-anatase mixed-phase TiO₂ with higher photocatalytic activity than the pure anatase or pure rutile phase TiO₂ has been attributed to the staggered energy band alignment at the *anatase*/rutile interface [41]. Similarly, SnO₂ with suitable conduction and valence band edge potentials can form a staggered energy band alignment with anatase or rutile TiO₂. It is expected that placing a thin SnO₂ layer in between the TiO₂ and high work function metal can effectively improve the separation of the photogenerated electron-hole pairs. In this study, a thin SnO₂ layer was placed in between the TiO₂ and Ni metal films to alleviate the recombination issue. The results show that with the appropriate band alignment of the heterojunction TiO₂/SnO₂/Ni, the photocatalytic activity of TiO₂ films has been highly improved.

2. Results and Discussion

Besides the heterojunction, the structure and surface roughness also affect the photocatalytic activity of TiO₂ films. Therefore, we first describe the structure and surface roughness of TiO₂ films grown on the chosen substrates of blank glass, Ni/Ti coated glass, SnO₂ coated glass and SnO₂/Ni/Ti

coated glass. Then, the measured photocatalytic activity of TiO₂ films is rendered and the junctions of TiO₂/Ni, TiO₂/SnO₂ and TiO₂/SnO₂/Ni on the photocatalytic activity of TiO₂ films are discussed.

Figure 1a,b show the XRD patterns of TiO₂ films grown on the blank glass, Ni/Ti coated glass, SnO₂ coated glass and the SnO₂/Ni/Ti coated glass at 250 and 350 °C, respectively. For the deposition temperature of 250 °C the films grown on the blank glass, Ni/Ti coated glass and SnO₂ coated glass are all crystallized in anatase form, but those grown on SnO₂/Ni/Ti coated glass are a mixture of anatase and rutile. As the deposition temperature is raised to 350 °C, the structure of TiO₂ films grown on the blank glass and SnO₂ coated glass become a mixture of anatase and rutile, but the structure of TiO₂ films grown on the Ni/Ti coated glass become an almost pure rutile. The TiO₂ films grown on the SnO₂/Ni/Ti coated glass, however, still maintain the anatase-rutile mixed structure. Apparently, the structure of TiO₂ films is related to both the deposition temperature and the substrate material. The SnO₂/Ni/Ti composite layer tends to enhance the formation of the rutile phase at a low temperature, but the Ni/Ti composite layer facilitates to the formation of pure rutile film at a relatively higher deposition temperature. The values of the surface roughness of these TiO₂ films are summarized in Table 1. For a given deposition temperature, the films grown on SnO₂/Ni/Ti coated glass have the roughest surface, followed by the films grown on blank glass, then the films grown on SnO₂ coated glass, and then the films grown on Ni/Ti coated glass. For a selected substrate, however, the films grown at 350 °C are rougher than the films grown at 250 °C.

Table 1. Surface roughness of TiO₂ films for the same samples in Figure 1.

Underlying Materials	Blank Glass		Ni/Ti Coated Glass		SnO ₂ Coated Glass		SnO ₂ /Ni/Ti Coated Glass	
	250	350	250	350	250	350	250	350
TiO ₂ deposition temperature (°C)	250	350	250	350	250	350	250	350
R _a of deposited TiO ₂ film (nm)	5.1	8.2	2.4	3.0	3.4	5.2	6.5	8.9

The photocatalytic activities of the TiO₂ films grown at 250 °C are shown in Figure 2. As expected, the SnO₂/Ni underlying layer performs far better than the SnO₂ and Ni underlying layers for improving the photocatalytic activity of TiO₂ films. However, it is interesting that the SnO₂ underlying layer has similar ability to the Ni underlying layer for improving the photocatalytic activity of TiO₂ films. Because the TiO₂ films on the Ni/Ti and SnO₂ coated glass have the same structure of anatase form as those on the blank glass but with a lower surface roughness, the mechanism of improvement in the photocatalytic activity of TiO₂ films by the Ni and SnO₂ underlying layers can be concluded to be the heterojunction of TiO₂/Ni and TiO₂/SnO₂. Without the effect of heterojunction, the TiO₂ films on the Ni or SnO₂ should have lower photocatalytic activity than on blank glass because of their lower surface roughness.

The improvement in photocatalytic activity of TiO₂ films by the Ni underlying layer can be described by the mechanism of Schottky-contact assisted carrier separation. The Ni has a work function of ~5.04–5.35 eV, and the TiO₂ has a conduction band minimum of ~−4.21 eV [42]. The junction of Ni with TiO₂ will exist a Schottky barrier. Figure 3 shows the I-V characteristics of the ALD TiO₂ on Ni. The diode behavior verifies the Schottky junction of Ni with TiO₂. As the band diagram of TiO₂/Ni shown in Figure 4, when the TiO₂ is irradiated with an intense UV light, a large amount of electron-hole pairs will be created and then the electron carriers in TiO₂ will flow to the Ni layer as depicted in Figure 4. As the photogenerated electron-hole pairs are separated, the Schottky barrier at the interface will block the photogenerated electrons from backing to the TiO₂, leaving the photogenerated holes, which have been considered to be the rate limiting carrier for methylene blue photooxidation in TiO₂. It is why the TiO₂/Ni heterojunction can improve the photocatalytic activity of TiO₂ films.

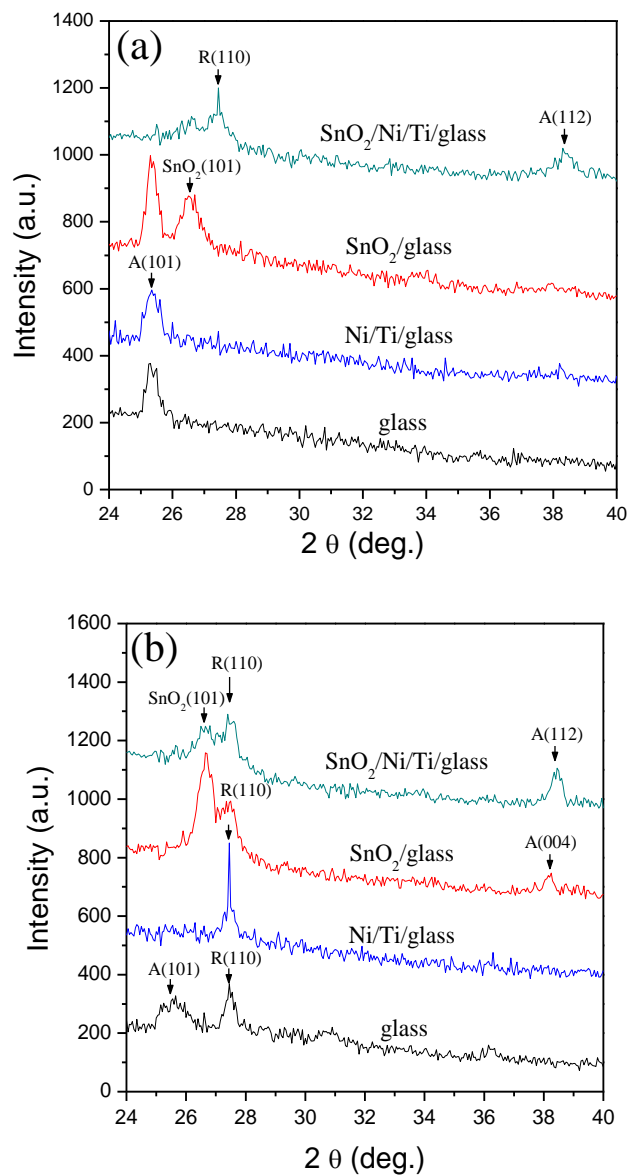


Figure 1. XRD patterns of TiO₂ films grown at (a) 250 °C and (b) 350 °C on various indicated underlying materials. The peak A and R indicate anatase and rutile TiO₂, respectively.

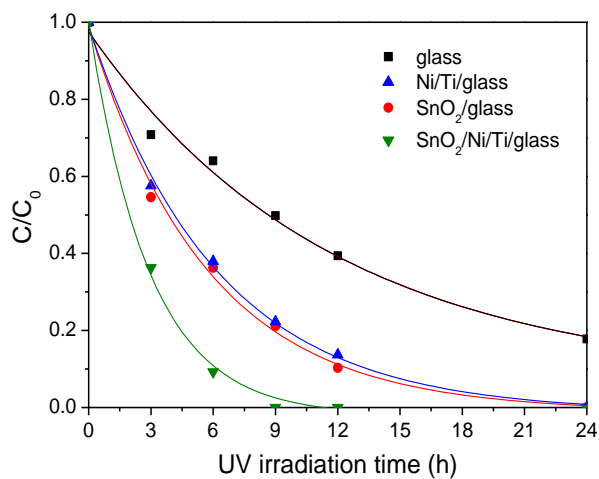


Figure 2. Residual MB concentration (C/C_0) versus UV irradiation time for characterizing photocatalysis of 250 °C-deposited TiO₂ films on various indicated underlying materials.

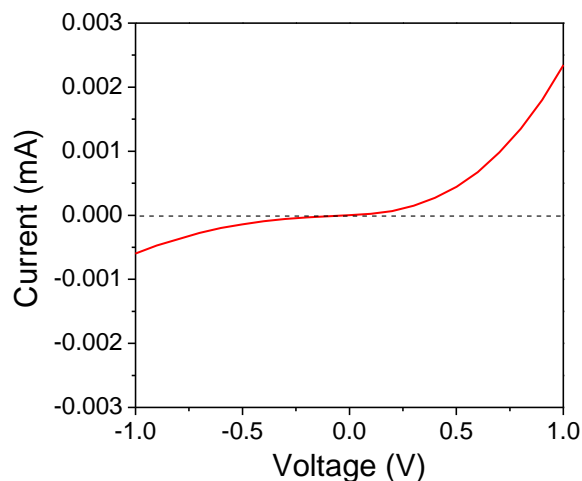


Figure 3. Current-voltage characteristic curve of TiO₂-Ni junction.

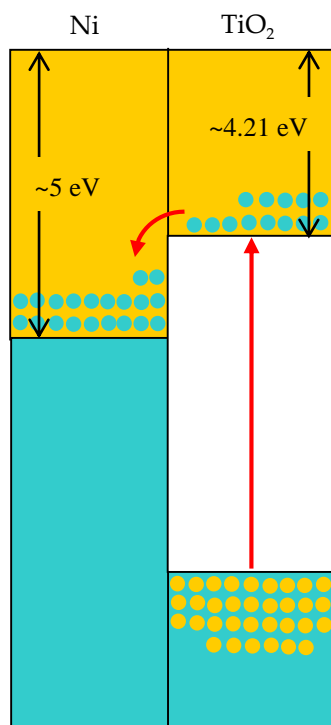


Figure 4. Schematic energy band diagrams of TiO₂/Ni heterojunction with electron-hole pairs separation mechanism after UV light irradiation.

The mechanism of TiO₂/Ni Schottky-contact assisted carrier separation was further verified by the dependence of the photocatalytic activity of TiO₂ films on the thickness of Ni underlying layer. Figure 5 shows the photocatalytic activities of TiO₂ films on the Ni/Ti coated glass with Ni thicknesses of 25, 50 and 100 nm, and Figure 6 is the extracted MB decay constants from the curves in Figure 5. The photocatalytic activity of TiO₂ film increases with the increase of Ni layer thickness but becomes saturated at a certain thickness. This result coincides with the mechanism described above. The thicker the Ni layer, the more low energy states in Ni for receiving the photogenerated electrons from TiO₂, leading to higher carrier separation efficiency. However, as the Ni layer is thick enough to receive most of the photogenerated electrons in TiO₂, the photocatalytic activity of TiO₂ film would become less dependent on the thickness of Ni layer.

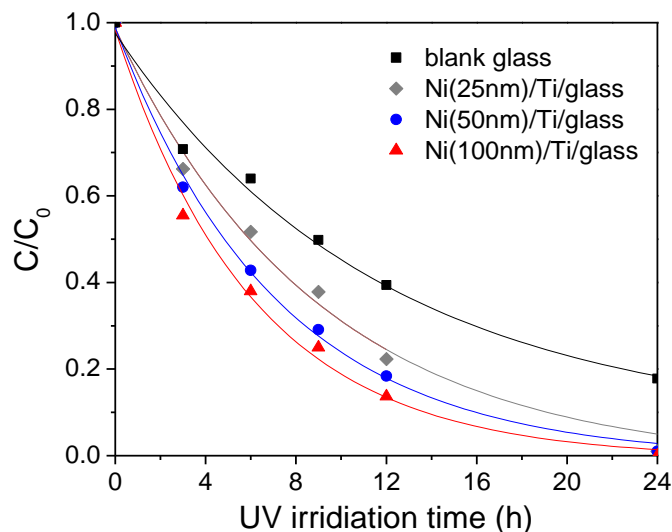


Figure 5. Residual MB concentration (C/C_0) versus UV irradiation time for characterizing photocatalysis of 250 °C-deposited TiO₂ films on blank glass and Ni/Ti coated glass with indicated Ni layer thickness.

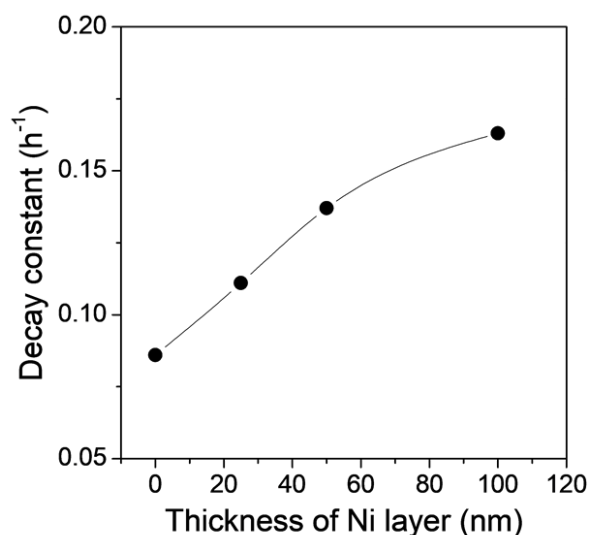


Figure 6. Dependence of MB decay constant on the thickness of Ni underlying layer for anatase TiO₂ films grown on Ni/Ti coated glass. The data are extracted from curves in Figure 4.

The improvement in the photocatalytic activity of TiO₂ films by the SnO₂ underlying layer is, however, due to the carrier separation assisted by staggered band alignment. SnO₂ is also an inherent n-type semiconductor with a conduction band minimum of ~ -4.50 eV and a band gap of ~ 3.67 eV [43]. In this work the carrier concentration in the SnO₂ measured by 4-point probe is as high as $\sim 10^{21}$ cm⁻³ which makes the Fermi level close to the conduction band minimum. Like the TiO₂/Ni junction, the TiO₂/SnO₂ junction is also favorable for the separation of photogenerated electron-hole pairs as shown in Figure 7. Despite the same features of TiO₂/Ni and TiO₂/SnO₂ junctions for carrier separation, two differences exist between them. One is that the available low energy states in SnO₂ are less than in Ni for receiving the photogenerated electrons from TiO₂; that is, the Ni underlying layer is more conductive than the SnO₂ underlying layer to the separation of photogenerated carriers in TiO₂. The other is that the TiO₂/SnO₂ junction has a higher barrier to hinder the diffusion of photogenerated holes from TiO₂ into SnO₂; that is, the SnO₂ underlying layer is more able than the Ni underlying layer to avoid recombination of the separated carriers. The combination of the two differences may be the

reason for the similar ability to improve the photocatalytic activity of TiO₂ films for both SnO₂ and Ni underlying layers.

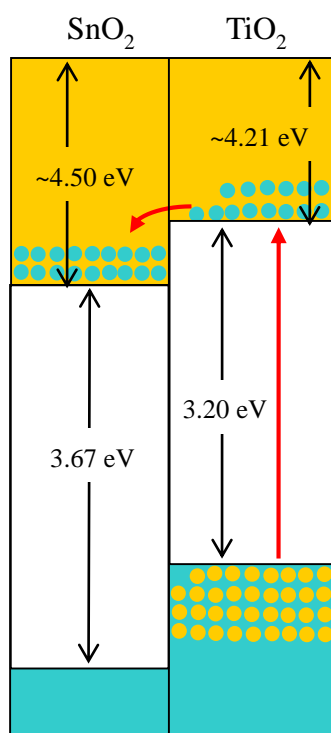


Figure 7. Schematic energy band diagrams of TiO₂/SnO₂ heterojunction showing the electron-hole separation mechanism after UV light irradiation.

The advantages of the high Schottky barrier of the TiO₂/Ni junction and the high hole diffusion barrier of TiO₂/SnO₂ junction can be incorporated together by inserting a thin SnO₂ layer in between TiO₂ and Ni. Figure 8 shows that the energy band diagram of TiO₂/SnO₂/Ni multi-junctions. The multi-junctions result in a staggered valence band alignment to block the holes from diffusing into the Ni layer and simultaneously keep the band bending structure for driving the electrons to the Ni layer. Thus the photogenerated electron-hole pairs are efficiently separated, and the separated carriers are isolated by a distance of SnO₂ layer from recombination at the interface. The low carrier recombination rate for TiO₂/SnO₂/Ni multi-heterojunctions is verified by the PL spectra shown in Figure 9. The PL intensity of TiO₂ film on SnO₂/Ni is less than one-fifteenth of that on Ni, indicating that placing the SnO₂ layer in between TiO₂ and Ni layers highly reduces the recombination of photogenerated carriers in TiO₂. It is considered to be the reason for the TiO₂ films grown on the SnO₂/Ni/Ti underlying layer with the best photocatalytic activity. However, the photocatalytic activity is also a function of the crystalline structure and surface roughness. The TiO₂ films on the SnO₂/Ni/Ti coated glass have a mixture of anatase and rutile structures, which is different from the pure anatase structure of TiO₂ films on SnO₂ or Ni/Ti coated glass. Moreover, the TiO₂ films on the SnO₂/Ni/Ti coated glass have a higher surface roughness than those on the SnO₂ or Ni/Ti coated glass. Both factors beneficial to the photocatalytic activity of TiO₂ films have been reported. Therefore, to identify this conclusion, it is necessary to further investigate the photocatalytic activity of TiO₂ films with the same structure and the same surface roughness on these underlying layers. Unfortunately, it is difficult to get TiO₂ films with the same structure and the same surface roughness on the SnO₂/Ni/Ti coated glass and on the SnO₂ or Ni/Ti coated glass. Out of compromise, the films grown at 350 °C were investigated to further understand the effects of mixed structure and roughness on the photocatalytic activity of TiO₂ films.

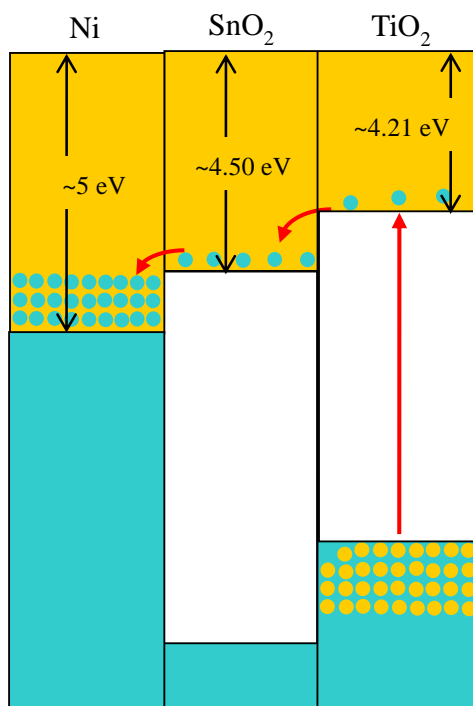


Figure 8. Schematic energy band diagrams of TiO₂/SnO₂/Ni multi-junctions showing the mechanism of efficient carrier separation.

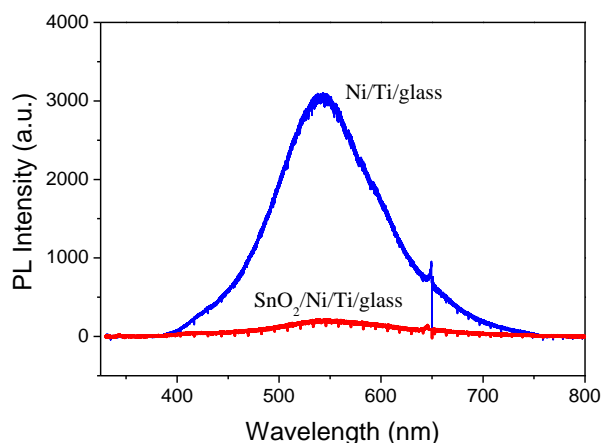


Figure 9. Photoluminescence spectra of TiO₂ films on Ni/Ti coated glass and on SnO₂/Ni/Ti coated glass under 325 nm excitation.

Figure 10 shows the photocatalytic activities of TiO₂ films grown on those underlying layers at 350 °C. Interestingly, compared with 250 °C the photocatalytic activity of the TiO₂ films grown on the SnO₂/Ni/Ti coated glass increased slightly, but the photocatalytic activity of the TiO₂ films grown on the blank glass decreased slightly. Moreover, the photocatalytic activity of the TiO₂ films grown on the SnO₂ coated glass and the Ni/Ti coated glass drops dramatically. From the results of XRD in Figure 1, the structure of TiO₂ films grown on the blank glass and SnO₂ coated glass changes from pure anatase to a mixture of anatase and rutile as the deposition temperature increases from 250 to 350 °C. The results in Figure 10 seem contradictory to the report that the TiO₂ with rutile-anatase mixed phases has higher photocatalytic activity than those with pure anatase or rutile phase. The contradiction was also found in our previous studies of TiO₂ films grown on Ni and Ta underlying layers that the photocatalytic activity of TiO₂ films decreases when the film structure changes from pure anatase to a mixture of anatase and rutile [38]. Although the fundamentals are still under investigation, this phenomenon indicates a high carrier recombination occurring in our

rutile-anatase mixed-phase films. The most plausible reason for the decrease is that the separated carriers recombine at the interfaces of rutile/anatase, rutile/SnO₂ and rutile/Ni. Despite the fact that these junctions can separate the photogenerated electron-hole pairs, the separated electrons and holes are able to recombine through the defects at the interface. In addition, the lower oxidizing power of rutile TiO₂ compared to anatase TiO₂ may result in a pileup of hole carriers in rutile and thus a more serious interface recombination.

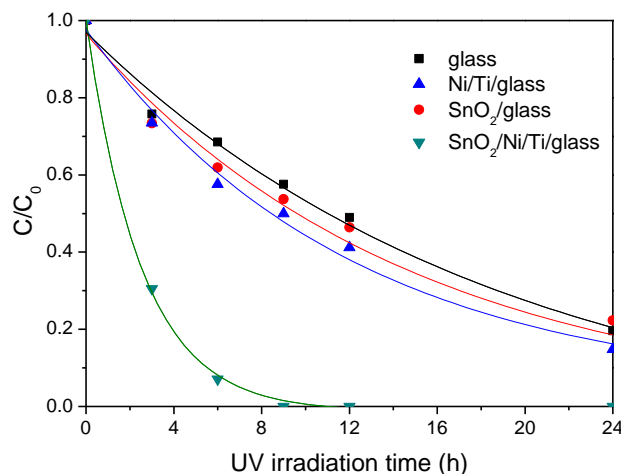


Figure 10. Residual MB concentration (C/C_0) versus UV irradiation time for characterizing photocatalysis of 350 °C-deposited TiO₂ films on various indicated underlying materials.

In contrast, the SnO₂ interlayer between Ni and TiO₂ can separate the electrons from holes by a distance of SnO₂ layer to avoid the recombination at the rutile-SnO₂ interface. Therefore, the TiO₂ films grown on SnO₂/Ni/Ti coated glass possess high photocatalytic activity even if they have the anatase-rutile mixed-phase structure. Furthermore, the 350 °C-deposited film has a slightly higher surface roughness than the 250 °C-deposited film, resulting in a slightly higher photocatalytic activity. The results in Figure 10 verify the conclusion that the high photocatalytic activity of TiO₂ films grown on SnO₂/Ni/Ti coated glass is due to the TiO₂/SnO₂/Ni multi-junctions rather than the anatase-rutile mixed-phase structure or the surface roughness. It is worth nothing that besides application for the photocatalysis, the high carrier separation ability of the multi-junctions can also be applied to other devices such as solar cells.

3. Experimental Section

Corning E2000 glass sheet with dimension of 3 × 2.5 cm² was used as the substrate for the deposition of various thin films. Four kinds of film configurations, namely TiO₂, TiO₂/SnO₂, TiO₂/Ni/Ti and TiO₂/SnO₂/Ni/Ti, were adopted in this study. The use of the Ti layer with a fixed thickness of ~30 nm was to improve the adhesion of the Ni layer to the glass substrate. The adoption of Ni layer is due to its high work function and low cost compared to the noble metals such as Ag, Au and Pt. The thickness of Ni layer was fixed at ~50 nm except for the samples to evaluate the effect of TiO₂/Ni heterojunction on the separation of photogenerated carriers in TiO₂. The adoption of the SnO₂ layer was because of its appropriate energy band structure which has higher valence band edge potential than TiO₂ for blocking the holes from entering into the Ni layer and higher electron affinity to catch electrons from TiO₂ [41]. Before the film deposition, the glass substrates were ultrasonically cleaned by acetone, methanol and DI water for 5 min in each step, and then dried by nitrogen purge gas. The Ti and Ni layers were grown by E-beam evaporator, and the SnO₂ and TiO₂ layers were grown by atomic layer deposition (ALD). SnCl₄ and TiCl₄ were used as the precursors of Sn and Ti for the ALD SnO₂ and ALD TiO₂, respectively, H₂O was used as the oxygen source and Ar gas as the purge gas. Each cycle of ALD SnO₂ (TiO₂) includes four steps of SnCl₄ (TiCl₄) pulse with 1 s, Ar purge

with 2 s, H₂O pulse with 1 s and Ar purge with 2 s. The SnO₂ films were deposited at 300 °C, and the TiO₂ films were grown at 250 and 350 °C. The deposition cycle for both the ALD SnO₂ and ALD TiO₂ was 1000, yielding a film thickness of ~52 nm for SnO₂ and ~55 nm for TiO₂.

The conductivity of Ni/Ti and SnO₂ layers was characterized by 4-point probe. The thickness of Ni/Ti layers was determined by profilometer, and the thickness of SnO₂ and TiO₂ layers was determined by ellipsometer. The surface roughness of films was measured by atomic force microscope. The crystalline structures of deposited films were identified by a grazing incident X-ray diffractometer with a voltage of 40 kV and a current of 40 mA at a wavelength of 1.5418 Å. The photoluminescence (PL) of TiO₂ on Ni and SnO₂/Ni coated glass was recorded using a He-Cd laser of 325 nm wavelength as the excitation source at room temperature. The photocatalytic activity of TiO₂ films was evaluated by measuring the degradation of methylene blue (MB) under UV-light irradiation at room temperature. Three 10 W of Sankyo Denki blacklight lamps with a center wavelength at 352 nm in parallel were used as the UV light sources. The samples were placed at the bottom of the glass cells (50 × 40 × 50 mm³ internal dimensions) filled with the MB solution of concentrations of 10⁻⁵ mol L⁻¹ with the height of 10 mm. The measured irradiation intensity at the film surface was 0.59 mW cm⁻², which is relatively low compared with others [44,45] in order to prevent the MB diffusion in the solution from becoming a limitation factor for the photocatalysis experiment. According to the Beer-Lambert law, the absorbance peak intensity of MB solution at 668 nm is proportional to the MB concentration, so that can be used to monitor the degradation of MB solution. The decrease of the absorbance of MB solutions was measured by a spectrometer at fixed intervals, and the residual MB concentration (C/C_0) was extracted by the change of absorbance at 668 nm. The photocatalytic degradation of MB can be described by an exponential decay function

$$C(t) = C_0 e^{-kt},$$

where C_0 and $C(t)$ is the MB concentration of initial and after exposure time t , and k is the exponential decay constant or photocatalytic activity.

4. Conclusions

TiO₂ films with thickness of ~55 nm were grown on blank glass, Ni/Ti coated glass, SnO₂ coated glass and SnO₂/Ni/Ti coated glass. The photocatalytic activity of these TiO₂ films was evaluated by measuring the MB degradation rate under irradiation of 352 nm UV light at room temperature. The results demonstrate that all the underlying layers of Ni, SnO₂ and SnO₂/Ni can improve the photocatalytic activity of the deposited TiO₂ films. Among them, the SnO₂/Ni underlying layer performs the best. The photocatalytic activity of TiO₂ films improved by Ni underlying layer and SnO₂ underlying layer is due to the Schottky barrier and staggered band alignment at the TiO₂/Ni and TiO₂/SnO₂ interfaces, respectively. However, the single junction of TiO₂/Ni or TiO₂/SnO₂ cannot avoid the carrier recombination at the interface. The multi-junctions of TiO₂/SnO₂/Ni can further separate the photogenerated electrons from holes by a distance of SnO₂ layer to avoid the recombination of separated carriers, and thus the photocatalytic activity of TiO₂ films is highly improved.

Author Contributions: H.-E.C. conceived and designed the experiments; C.-H.H. performed the experiments; H.-E.C., I.-S.Y. and Z.-P.Y. analyzed the data; H.-E.C. and Z.-P.Y. wrote the paper.

Acknowledgments: The authors would like to thanks the financial support from Ministry of Science and Technology (contract no. MOST 105-2221-E-218-001 and MOST 106-2221-E-009-122-MY3).

Conflicts of Interest: The authors declare no conflict of interest.

References

1. Kulkarni, M.; Mazare, A.; Gongadze, E.; Perutkova, S.; Kralj-Iglič, V.; Milošev, I.; Schmuki, P.; Igljic, A.; Mozetic, M. Titanium Nanostructures for Biomedical Applications. *Nanotechnology* **2015**, *26*, 062002. [[CrossRef](#)] [[PubMed](#)]

2. Zhao, X.B.; Peng, C.; You, J.J. Plasma-Sprayed ZnO/TiO₂ Coatings with Enhanced Biological Performance. *Therm. Spray Technol.* **2017**, *26*, 1301–1307. [[CrossRef](#)]
3. Wang, J.X.; Wang, L.T.; Fan, Y.B. Adverse Biological Effect of TiO₂ and Hydroxyapatite Nanoparticles Used in Bone Repair and Replacement. *Int. J. Mol. Sci.* **2016**, *17*, 798. [[CrossRef](#)] [[PubMed](#)]
4. Bonetta, S.; Bonetta, S.; Motta, F.; Strini, A.; Carraro, E. Photocatalytic Bacterial Inactivation by TiO₂-Coated Surfaces. *AMB Express* **2013**, *3*, 59. [[CrossRef](#)] [[PubMed](#)]
5. Gupta, K.; Singh, R.P.; Pandey, A.; Pandey, A. Photocatalytic Antibacterial Performance of TiO₂ and Ag-Doped TiO₂ against *S. Aureus*, *P. Aeruginosa* and *E. Coli*. *J. Nanotechnol.* **2013**, *4*, 345–351.
6. Yates, M.H.; Brook, L.A.; Ditta, I.B.; Evans, P.; Foster, A.H.; Sheel, W.D.; Steele, A. Photo-Induced Self-Cleaning and Biocidal Behaviour of Titania and Copper Oxide Multilayers. *J. Photochem. Photobiol. A* **2008**, *197*, 197–205. [[CrossRef](#)]
7. Zhang, L.; Dillert, R.; Bahnemann, D. Photoinduced Hydrophobicity and Self-Cleaning: Models and Reality. *Energy Environ. Sci.* **2012**, *5*, 7491–7507. [[CrossRef](#)]
8. Fujishima, A.; Zhang, X.; Tryk, D.A. TiO₂ Photocatalysis and Related Surface Phenomena. *Surf. Sci. Rep.* **2008**, *63*, 515–582. [[CrossRef](#)]
9. Cheng, H.-E.; Chen, C.-C. Morphological and Photoelectrochemical Properties of ALD TiO₂ Films. *J. Electrochem. Soc.* **2008**, *155*, D604–D607. [[CrossRef](#)]
10. Chen, J.; Qiu, F.; Xu, W.; Cao, S.; Zhu, H. Recent Progress in Enhancing Photocatalytic Efficiency of TiO₂-Based Materials. *Appl. Catal. A* **2015**, *495*, 131–140. [[CrossRef](#)]
11. Sakata, T. *Photocatalysis: Fundamentals and Applications*; Serpone, N., Pelizzetti, E., Eds.; John Wiley & Sons: New York, NY, USA, 1989; p. 314.
12. Yang, G.; Ding, H.; Feng, J.; Hao, Q.; Sun, S.; Ao, W.; Chen, D. Highly Performance Core-Shell TiO₂(B)/anatase Homo Junction Nanobelts with Active Cobalt phosphide Cocatalyst for Hydrogen Production. *Sci. Rep.* **2017**, *7*, 14594. [[CrossRef](#)] [[PubMed](#)]
13. Preethi, L.K.; Antony, R.P.; Mathews, T.; Walczak, L.; Gopinath, C.S. A Study on Doped Heterojunctions in TiO₂ Nanotubes: An Efficient Photocatalyst for Solar Water Splitting. *Sci. Rep.* **2017**, *7*, 14314. [[CrossRef](#)] [[PubMed](#)]
14. Sorathiya, K.; Mishra, B.; Kalarikkal, A.; Reddy, K.P.; Gopinath, C.S.; Khushalani, D. Enhancement in Rate of Photocatalysis Upon Catalyst Recycling. *Sci. Rep.* **2016**, *6*, 35075. [[CrossRef](#)] [[PubMed](#)]
15. Tugaoen, H.O.; Garcia-Segura, S.; Hristovski, K.; Westerhoff, P. Challenges in Photocatalytic Reduction of Nitrate as a Water Treatment Technology. *Sci. Total Environ.* **2017**, *599*, 1524–1551. [[CrossRef](#)] [[PubMed](#)]
16. Tsai, C.Y.; Liu, C.W.; Chan, Y.H.; Chang, T.Y.; Chen, B.C.; Hsi, H.C. Development of HCl-Treated Titania Nanotubes Photocatalysts for Dye Photodegradation and Low-Concentration Elemental Mercury Removal. *Catal. Today* **2017**, *297*, 113–123. [[CrossRef](#)]
17. Chang, L.H.; Cho, C.P. Exploration of Silver Decoration Concentration to Enhance Photocatalytic Efficiency of Titanium Dioxide Photocatalysts. *Solid State Sci.* **2016**, *62*, 112–120. [[CrossRef](#)]
18. Yu, J.C.C.; Nguyen, V.H.; Lasek, J.; Wu, J.C.S. Titania Nanosheet Photocatalysts with Dominantly Exposed (001) Reactive Facets for Photocatalytic NO_x Abatement. *Appl. Catal. B* **2017**, *219*, 391–400. [[CrossRef](#)]
19. Ohno, T.; Sarukawa, K.; Tokieda, K.; Matsumura, M. Morphology of a TiO₂ Photocatalyst (Degussa, P-25) Consisting of Anatase and Rutile Crystalline Phases. *J. Catal.* **2001**, *203*, 82–86. [[CrossRef](#)]
20. Luttrell, T.; Halpegamage, S.; Tao, J.; Kramer, A.; Sutter, E.; Batzill, M. Why is Anatase a Better Photocatalyst than Rutile?—Model Studies on Epitaxial TiO₂ Films. *Sci. Rep.* **2014**, *4*, 4043. [[CrossRef](#)] [[PubMed](#)]
21. Macak, J.M.; Ghicov, A.; Hahn, R.; Tsuchiya, H.; Schmuki, P. Photoelectrochemical Properties of N-Doped Self-Organized Titania Nanotube Layers with Different Thicknesses. *J. Mater. Res.* **2006**, *21*, 2824–2828. [[CrossRef](#)]
22. Zhang, Y.Y.; Gu, D.; Zhu, L.Y.; Wang, B.H. Highly Ordered Fe³⁺/TiO₂ Nanotube Arrays for Efficient Photocatalytic Degradation of Nitrobenzene. *Appl. Surf. Sci.* **2017**, *420*, 896–904. [[CrossRef](#)]
23. Liu, C.-M.; Chen, C.; Cheng, H.-E. Ultraviolet Photoresponse of TiO₂ Nanotube Arrays Fabricated by Atomic Layer Deposition. *Electrochem. Solid-State Lett.* **2011**, *14*, K33–K35. [[CrossRef](#)]
24. Cheng, H.-E.; Lin, C.-Y.; Hsu, C.-M. Fabrication of SnO₂-TiO₂ Core-Shell Nanopillar-Array Films for Enhanced Photocatalytic Activity. *Appl. Surf. Sci.* **2017**, *396*, 393–399. [[CrossRef](#)]
25. Jia, L.; Qiu, J.C.; Du, L.Q.; Li, Z.; Liu, H.; Ge, S.H. TiO₂ Nanorod Arrays as a Photocatalytic Coating Enhanced Antifungal and Antibacterial Efficiency of Ti Substrates. *Nanomedicine* **2017**, *12*, 761–776. [[CrossRef](#)] [[PubMed](#)]

26. Han, Y.H.; Zhang, L.; Wang, Y.F.; Zhang, H.M.; Zhang, S.Q. Photoelectrocatalytic Activity of an Ordered and Vertically Aligned TiO₂ Nanorod Array/BDD Heterojunction Electrode. *Sci. Bull.* **2017**, *62*, 619–625. [[CrossRef](#)]
27. Zhang, Q.J.; Fu, Y.; Wu, Y.F.; Zuo, T.Y. Lanthanum-Doped TiO₂ Nanosheet Film with Highly Reactive {001} Facets and Its Enhanced Photocatalytic Activity. *Eur. J. Inorg. Chem.* **2016**, *11*, 1706–1711. [[CrossRef](#)]
28. Nair, A.K.; JagadeeshBabu, P.E. TiO₂ Nanosheet-Graphene Oxide Based Photocatalytic Hierarchical Membrane for Water Purification. *Surf. Coat. Technol.* **2017**, *320*, 259–262. [[CrossRef](#)]
29. Wei, N.; Cui, H.Z.; Song, Q.; Zhang, L.Q.; Song, X.J.; Wang, K.; Zhang, Y.F.; Li, J.; Wen, J.; Tian, J. Ag₂O Nanoparticle/TiO₂ Nanobelt Heterostructures with Remarkable Photoresponse and Photocatalytic Properties under UV, Visible and Near-Infrared Irradiation. *Appl. Catal. B* **2016**, *198*, 83–90. [[CrossRef](#)]
30. Lai, L.L.; Wu, J.M. A Facile Solution Approach to W,N Co-doped TiO₂ Nanobelt Thin Films with High Photocatalytic Activity. *J. Mater. Chem. A* **2015**, *3*, 15863–15868. [[CrossRef](#)]
31. Trabelsi, K.; Hajjaji, A.; Gaidi, M.; Bessais, B.; El Khakani, M.A. Enhancing the Photoelectrochemical Response of TiO₂ Nanotubes through Their Nanodecoration by Pulsed-Laser-Deposited Ag Nanoparticles. *J. Appl. Phys.* **2017**, *122*, 064503. [[CrossRef](#)]
32. Shuang, S.; Lv, R.T.; Xie, Z.; Zhang, Z.J. Surface Plasmon Enhanced Photocatalysis of Au/Pt-Decorated TiO₂ Nanopillar Arrays. *Sci. Rep.* **2016**, *6*, 26670. [[CrossRef](#)] [[PubMed](#)]
33. Cui, W.Y.; Xue, D.; Yuan, X.L.; Zheng, B.; Jia, M.J.; Zhang, W.X. Acid-Treated TiO₂ Nanobelt Supported Platinum Nanoparticles for the Catalytic Oxidation of Formaldehyde at Ambient Conditions. *Appl. Surf. Sci.* **2017**, *411*, 105–112. [[CrossRef](#)]
34. Chen, J.-J.; Wang, W.-K.; Li, W.-W.; Pei, D.-N.; Yu, H.-Q. Roles of Crystal Surface in Pt-Loaded Titania for Photocatalytic Conversion of Organic Pollutants: A First-Principle Theoretical Calculation. *ACS Appl. Mater. Interfaces* **2015**, *7*, 12671–12678. [[CrossRef](#)] [[PubMed](#)]
35. Momeni, M.M.; Ghayeb, Y. Photoinduced Deposition of Gold Nanoparticles on TiO₂-WO₃ Nanotube Films as Efficient Photoanodes for Solar Water Splitting. *Appl. Phys. A* **2016**, *122*, 620. [[CrossRef](#)]
36. Marelli, M.; Evangelisti, C.; Diamanti, M.V.; Dal Santo, V.; Pedefferri, M.P.; Bianchi, C.L.; Schiavi, L.; Strini, A. TiO₂ Nanotubes Arrays Loaded with Ligand-Free Au Nanoparticles: Enhancement in Photocatalytic Activity. *ACS Appl. Mater. Interfaces* **2016**, *8*, 31051–31058. [[CrossRef](#)] [[PubMed](#)]
37. Wang, H.L.; Liu, X.H. Preparation of Silver Nanoparticle Loaded Mesoporous TiO₂ and Its Photocatalytic Property. *J. Inorg. Mater.* **2016**, *31*, 555–560.
38. Cheng, H.-E.; Hsu, C.-M.; Chen, Y.-C. Substrate Materials and Deposition Temperature Dependent Growth Characteristics and Photocatalytic Properties of ALD TiO₂ Films. *J. Electrochem. Soc.* **2009**, *156*, D275–278. [[CrossRef](#)]
39. 39. In *CRC Handbook of Chemistry and Physics*; CRC Press: Boca Raton, FL, USA, 2008; pp. 12–114.
40. Miyauchi, M.; Nakajima, A.; Watanabe, T.; Hashimoto, K. Photoinduced Hydrophilic Conversion of TiO₂/WO₃ Layered Thin Films. *Chem. Mater.* **2002**, *14*, 4714–4720. [[CrossRef](#)]
41. Scanlon, D.O.; Dunnill, C.W.; Buckeridge, J.; Shevlin, S.A.; Logsdail, A.J.; Woodley, S.M.; Catlow, C.R.A.; Powell, M.J.; Palgrave, R.G.; Parkin, I.P.; et al. Band Alignment of Rutile and Anatase TiO₂. *Nat. Mater.* **2013**, *12*, 798–801. [[CrossRef](#)] [[PubMed](#)]
42. Xu, X.; Schoonen, M.A.A. The Absolute Energy Positions of Conduction and Valence Bands of Selected Semiconducting Minerals. *Am. Mineral.* **2000**, *85*, 543–556. [[CrossRef](#)]
43. Ganose, A.M.; Scanlon, D.O. Band Gap and Work Function Tailoring of SnO₂ for Improved Transparent Conducting Ability in Photovoltaics. *J. Mater. Chem. C* **2016**, *4*, 1467–1475. [[CrossRef](#)]
44. Lamberti, A.; Chiodoni, A.; Shahzad, N.; Bianco, S.; Quaglio, M.; Pirri, C.F. Ultrafast Room-Temperature Crystallization of TiO₂ Nanotubes exploiting Water-Vapor Treatment. *Sci. Rep.* **2015**, *5*, 7808. [[CrossRef](#)] [[PubMed](#)]
45. Yaghoubi, H.; Taghavinia, N.; Alamdari, E.K. Self Cleaning TiO₂ Coating on Polycarbonate: Surface Treatment, Photocatalytic and Nanomechanical Properties. *Surf. Coat. Technol.* **2010**, *204*, 1562–1568. [[CrossRef](#)]

